
Interpreting a Recurrent Neural Network Model for ICU Mortality Using Learned Binary Masks

Long V. Ho

VPICU

Children’s Hospital Los Angeles
lho@chla.usc.edu

Melissa D. Aczon

VPICU

Children’s Hospital Los Angeles
maczon@chla.usc.edu

David Ledbetter

VPICU

Children’s Hospital Los Angeles
dledbetter@chla.usc.edu

Randall Wetzel

VPICU

Children’s Hospital Los Angeles
rwetzel@chla.usc.edu

Abstract

An attribution method was developed to interpret a recurrent neural network (RNN) trained to predict a child’s risk of ICU mortality using multi-modal, time series data in the Electronic Medical Records. By learning a sparse, binary mask that highlights salient features of the input data, critical features determining an individual patient’s severity of illness could be identified. The method, called Learned Binary Masks (LBM), demonstrated that the RNN used different feature sets specific to each patient’s illness; and further, the features highlighted aligned with clinical intuition of the patient’s disease trajectories. LBM was also used to identify the most salient features across model, analogous to “feature importance” computed in the Random Forest. This measure of the RNN’s feature importance was further used to select the 25% most used features for training a second RNN model. Interestingly, but not surprisingly, the second model maintained similar performance to the model trained on all features. LBM is data-agnostic and can be used to interpret the predictions of any differentiable model.

1 Introduction

Despite the widespread success of deep learning algorithms, acceptance has been impeded by their lack of transparency, especially in healthcare where decisions can result in life and death [1]. In response, research efforts to interpret these models have increased recently [2, 3, 4, 5, 6]. Olah et al. [7] establishes two major research areas in neural network interpretability: attribution and feature visualization. Attribution focuses on why the network made the predictions by identifying inputs that were salient for making the predictions [6]. Feature visualization addresses questions about the network by finding what concepts the model learned [8].

The majority of existing attribution approaches interpret neural networks by using derivatives. Attributions are visualized with respect to the inputs; for example, pixels are highlighted based on their rankings computed from the chosen attribution method. The application of these methods and visualizations of their results have mostly been limited to the domains of images and texts — single-sensor inputs [9]. In contrast, the Electronic Medical Records (EMR), a treasure trove of data capturing patient events, contain an eclectic collection of data ranging from continuous physiology (heart rate), categoricals (Glasgow Coma Score), binary (culture labs), and unstructured texts (clinical notes) [10]. Consequently, it is nontrivial how current attribution methods translate to multi-modal, time-series data contained in EMR; and further, how to analyze and visualize their results.

This work developed an attribution method for interpreting a recurrent neural network (RNN) model using multi-modal EMR data. In addition, the attributions are presented in a way such that visualizing and analyzing the breadth of information are intuitive and meaningful for clinicians. This ensures that practical users (clinicians) can gain confidence in the highly accurate, "black-box" model as well as receive relevant, actionable information at scale. The attribution method, called Learned Binary Masks, was used to interpret a RNN model trained to predict an individual child's risk of mortality using the patient's EMR.

2 Related Work

Saliency methods provide insights into the network's prediction by using the differentiability of neural networks [11]. A majority of applications of these methods have been limited to single-sensor inputs such as pixels in images and characters in text [9]. For example, they can highlight which pixels contributed to the model's belief that a specific class of interest was in the image [2, 3, 4, 5, 6]. Similarly, they can highlight which words in a sentence were most impactful to the model in determining the sentiment of a sentence or prediction of the next word [12, 13]. In both problems, they are typically visualized as heatmaps over the inputs, ranking pixels or characters in a word based on their impact on the prediction.

In contrast to these unimodal problems, EMR can span hundreds of features and data-modalities. For example, a heart rate may be measured every hour and stored as an integer ranging from 50 to 250 beats per minute, while pupil response may be measured every 4 hours and represented qualitatively as {Non-reactive, Pinpoint, or Brisk}. Comparisons and visualizations of attributions from multi-modal data are more complex — e.g. how does a gradient with respect to heart rate ($\partial y / \partial x, x \in [50, 250]$) compare with the gradient with respect to pupil response ($\partial y / \partial x, x \in \{\text{Non-reactive, Pinpoint, Brisk}\}$)?

The attribution method developed here extends the occlusion method in Fong and Vedaldi [5]. However, instead of learning a mask that optimally *deletes* information to reduce the class prediction to zero, a *binary* mask is learned that optimally *keeps* information required to generate the same prediction. The binary property of the mask ensures that attribution comparisons between multi-modal data simply indicate the salient variables used at each prediction.

3 Application: Dynamic Prediction of Risk of ICU Mortality using RNNs

Numerous severity of illness (SOI) and mortality scoring systems have emerged over the last three decades [14, 15, 16, 17]. Over many years, these systems have been refined with increasingly larger number of patients [18, 19, 20, 21, 22, 23]. Despite the number of SOI scores developed, their primary use have been limited to evaluating ICU (Intensive Care Unit) performance and selecting patient cohorts for clinical trials [24, 25, 26], instead of guiding treatments and interventions [27]. One reason for this is because the scores are not dynamic – they use features computed over fixed time windows of data (e.g. 12 hours of data from ICU admission) and generate a static risk of mortality (ROM) score at a single point in time (e.g. at the 12th hour). Another reason is because the predictions are merely descriptive – there is no accompanying attribution or reasoning for the models' individual patient predictions.

An RNN model was trained to predict ICU mortality and was the use case for the attribution method described in Section 4. The RNN generates a dynamic ROM score and can elegantly update its prediction as data is accrued. By using the attribution method, salient features unique to the patient can be highlighted, illuminating *why* the model made its prediction specific to that patient, and thus providing the clinician with actionable information. By understanding both *how* sick the patient is (model's prediction) and *why* they're sick (LBM attributions), clinicians can use this information to guide treatments and allocations of resources in real-time at the bedside.

De-identified patient EMR data collected in the Pediatric Intensive Care Unit (PICU) of a tertiary hospital was used. The data consisted of 9955 patient-encounters (7358 patients) admitted from 2009 to 2017 (4% mortality rate). Each patient-encounter contained irregularly sampled physiologic observations, laboratory results, drugs, and interventions (e.g. intubation parameters) over their ICU stay. Also collected were the patient's demographics, diagnoses, and outcomes (e.g. ICU mortality). The data was preprocessed as described in [28], resulting in a $T \times N$ matrix per patient (called

“patient-matrix”). $N = 270$ is the number of features (constant across all patients), while T is the number of distinct time points when a patient had a measurement (varies across patients). The features were chosen based on their frequency of measurement and relevance to the outcome. The chosen features are listed in Appendix B.

The patient-matrix is the input to a many-to-many RNN trained to predict an individual patient’s ROM. Each time step (column of patient-matrix) generates a ROM prediction. Training details such as the network architecture, hyper-parameters, and implementation are described in Appendix A. The model was evaluated using Area under the Receiver Operating Characteristic (AUROC) curve after 12 hours of measurements. This allowed for comparisons with SOI scores deployed in the pediatric ICU: PIM2 and PRISM3-12 [22, 20]. Three RNN models were trained with different initialized weights and sequencing of mini-batches. Their averaged 12th hour AUC (0.940 ± 0.004) significantly outperformed that of PIM2 (0.880) and PRISM3-12 (0.896).

4 Learned Binary Masks

A many-to-many RNN maps an input sequence, $\mathbf{x}_{1:T}$ (the patient-matrix), to an output sequence, $y_{1:T}$ (risk of mortality), of the same length:

$$f(\Theta; \mathbf{x}_{1:T}) = y_{1:T}, \quad (1)$$

where Θ denotes the parameters of the trained network f . LBM attributes the predictions to the input by finding a sparse binary mask, such that the trained network, when given the masked input, outputs the *same* prediction as the original input data. Mathematically, this is expressed by

$$f(\Theta; \mathbf{x}_{1:T} \odot \mathbf{m}_{1:T}) \approx f(\Theta; \mathbf{x}_{1:T}), \quad (2)$$

where $\mathbf{m}_{1:T} \in [0, 1]^{T \times N}$ is the learned mask applied to the input via element-wise matrix multiplication represented by \odot . This is implemented as a new layer to the trained network f . Let $\tilde{y}_{1:T} \equiv f(\Theta; \mathbf{x}_{1:T} \odot \mathbf{m}_{1:T})$ denote the output of the trained network when given the masked sequence as input. Then $\mathbf{m}_{1:T}$ is found by using backpropagation to minimize the loss function:

$$L(\mathbf{m}_{1:T}) = \sum_{t=1}^T |y(t) - \tilde{y}(t)| + \lambda_1 \|\mathbf{m}_{1:T}\|_1, \quad (3)$$

where λ_1 is a constant, and $\|\mathbf{m}_{1:T}\|_1 = \sum_{t=1}^T \sum_{j=1}^N |m_t^j|$. If the first term, $\sum_{t=1}^T |y_t - \tilde{y}_t|$, is zero, then the two output sequences ($y_{1:T}$ – generated by the original input sequence ($\mathbf{x}_{1:T}$), and $\tilde{y}_{1:T}$ – generated by the masked input sequence ($\mathbf{x}_{1:T} \odot \mathbf{m}_{1:T}$)), match each other. Minimizing the second term, $\lambda_1 \|\mathbf{m}_{1:T}\|_1$, encourages the mask $\mathbf{m}_{1:T}$ to be sparse, equivalent to asking that only the salient inputs be kept. If $m_t^j = 0$, then the j^{th} feature at time t can be set to zero without changing the output, i.e. m_t^j was not critical to making the prediction, and the population mean was sufficient information. If $m_t^j = 1$, then x_t^j was a critical measurement in the model’s prediction. On the other hand, if $m_t^j \in (0, 1)$, then $x_t^j \cdot m_t^j$ is a scaled value of x_t^j and no longer represents the presence or removal of the feature with respect to its contribution to the model’s prediction, which makes interpretation challenging.

4.1 Learned Binary Masks via 2-step Optimization

Comparing non-binary values of m_t^j poses interpretability challenges. Therefore, the algorithm is modified to enforce an additional constraint: the mask can take on only binary values, namely $m_t^j \in \{0, 1\}$. This constraint cannot be integrated into optimization methods that use derivatives such as backpropagation. Therefore, the algorithm is modified by using a 2-step optimization process. The first step uses backpropagation-optimization to find an initial mask whose values are close to 0 or 1. The second step fine-tunes the mask for interpretability by binarizing the mask using brute-force optimization. The initial mask is computed as described previously but augmented with additional conditions that optimize a mask with elements closer to 0 or 1.

Step 1: Find an initial mask $\mathbf{m}_{1:T} \in [0, 1]^{T \times N}$ using backpropagation.

Redefine $\tilde{y} \equiv f(\Theta; \mathbf{x}_{1:T} \odot \sigma(A \times \mathbf{m}_{1:T}))$, where $\sigma(x) = \frac{1}{1+e^{-x}}$, and A is a constant. The first mask $\mathbf{m}_{1:T}$ is computed by minimizing the loss function:

$$L(\mathbf{m}_{1:T}) = \sum_{t=1}^T |y(t) - \tilde{y}(t)| + \lambda_1^1 \|\mathbf{m}_{1:T}\|_1 + \lambda_2 H(\mathbf{m}_{1:T} > 0.5, \mathbf{m}_{1:T}) \quad (4)$$

where H is the binary cross-entropy function, and λ_2 is a constant. This loss function parallels equation 3, but adds a binary cross-entropy term to push the values of the mask closer to 0 or 1. The first term is augmented with the sigmoid function to further push the values modifying the inputs closer to 0 or 1. Equation 4, like Equation 3, can be minimized by using backpropagation mechanics.

Step 2: Binarize the initial mask $\mathbf{m}_{1:T} \in [0, 1]^{T \times N}$ using brute-force optimization.

The mask $\mathbf{m}_{1:T}$ is binarized by finding a threshold mask $\tau_{1:T}$ such that

$$f(\Theta; \mathbf{x}_{1:T} \odot (\mathbf{m}_{1:T} > \tau_{1:T})) \approx f(\Theta; \mathbf{x}_{1:T}). \quad (5)$$

Redefining $\tilde{y} \equiv f(\Theta; \mathbf{x}_{1:T} \odot (\mathbf{m}_{1:T} > \tau_{1:T}))$, then $\tau_{1:T}$ is found by minimizing the loss function:

$$L(\tau_{1:T}) = \sum_{t=1}^T |y(t) - \tilde{y}(t)| + \lambda_1^2 \|\mathbf{m}_{1:T} > \tilde{\tau}_{1:T}\|_1. \quad (6)$$

Equation 6 can be minimized using brute-force grid-search of threshold values $\tau_t^j \in [0, 1]$. The final result is a binary mask, $\mathbf{M}_{1:T} \equiv (\mathbf{m}_{1:T} > \tau_{1:T})$. The binary nature of each M_t^j indicates whether x_t^j was critical in making the prediction $\hat{y}_{1:T}$ and allows for comparisons between multi-modal input features.

4.2 Implementation Details

Learned Binary Masks was developed to interpret the RNN trained to predict ROM using EMR data. Although the notation used were specific to time-series data and RNNs, the technique is data-agnostic and can be applied to any differentiable model. LBM was implemented using keras, a high-level Python neural networks API [29]. The code will be made publicly available on GitHub.

Step 1's Equation 4 was minimized using RMSProp [30] with $\lambda_1^1 = 0.005$ and $\lambda_2 = 0.5$. The learning rate was initialized to 0.1 and reduced by 10 if it did not decrease after 5 iterations. Optimization is stopped if learning rate was reduced by 10 for a total of 3 decimations, or after 5000 iterations. Step 2's Equation 6 was minimized using brute-force grid search of $\tau_{1:T} \in [0, 1]^{T \times N}$ and $\lambda_1^2 = 10^{-4}$.

LBM is a computationally expensive 2-step optimization process applied to each patient. Moreover, because patients have variable sequence lengths, finding an optimal binary mask for each patient can vary widely. For reference, using a Titan V Volta GPU and keras with Theano-backend, it takes 0.01 seconds to generate predictions for a patient with 500 time steps and 270 features. On the other hand, it takes 30 minutes to compute LBM on the same data, which can be heavily improved but is still reasonable in application.

4.3 Interpreting Attributions

Understanding why a model predicted an increase in ROM from 0.1 to 0.9 is more useful than understanding why a model made a single ROM prediction of 0.9. LBM attributions can highlight what features contributed the most to the model's shift in prediction by computing the average LBM attribution over the time window of interest:

$$\overline{\mathbf{M}}_{t_i:t_f} \equiv \sum_{t=t_i}^{t_f} \mathbf{M}(t) / n(t_i, t_f), \quad (7)$$

where $n(t_i, t_f)$ is the number of time steps in the time interval $[t_i, t_f]$. $\overline{\mathbf{M}}_{t_i:t_f} \in \mathbb{R}^N$ is a vector describing the average use of each feature in making the prediction from $t = t_i$ to $t = t_f$.

Feature Importance An individual patient p has an associated attribution matrix $\mathbf{M}_{1:T_p}^p \in \mathbb{R}^{T_p \times N}$, where T_p is the total time steps for that patient's entire ICU stay. Setting $t_i = 1$ and $t_f = T_p$ in Equation 7 yields a vector containing the frequency that each feature was used by the model to generate this patient's ROM scores over their entire ICU stay. This vector, denoted by $\overline{\mathbf{M}}_{1:T_p}^p$, can be averaged over all P patients to yield a population-level feature contribution vector:

$$\mathbf{F} \equiv \sum_{p=1}^P \overline{\mathbf{M}}_{1:T_p}^p. \quad (8)$$

The vector $\mathbf{F} \in \mathbb{R}^N$ is analogous to “feature importance” computed in machine learning models such as the Random Forest [31]. Feature importance should be averaged over the population in the validation set, P_{valid} , because the training set is used for optimizing the weights and test set for performance analysis. In contrast to ranking features based on their direct effects on the model’s predictive performance, the LBM’s “feature importance” as computed above is a measure of how frequently the feature is required for making predictions, independent of whether it improves the model’s performance.

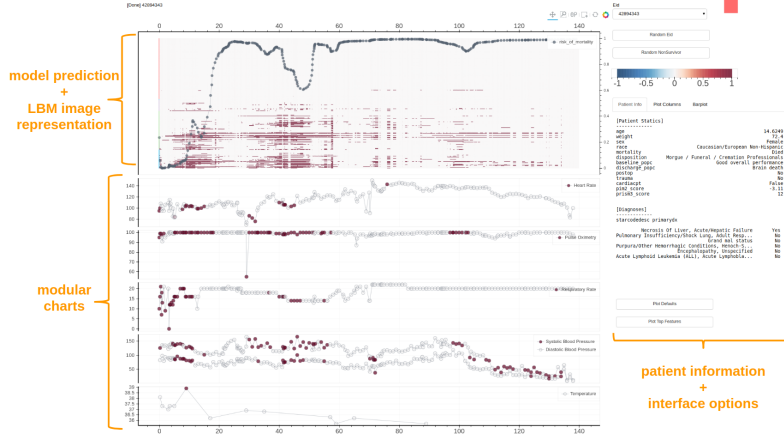


Figure 1: Example of the modular visualization interface for interpreting attributions alongside data.

4.4 Visualizing Attributions for Interpretation

On average, patients stay 4.5 days in the ICU with 230 unique time measurements. With over 270 features, visualizing the totality of an individual patient’s data can be overwhelming, let alone also visualizing the attribution matrices. Moreover, any visualization should be intuitive for clinicians and harmonize into their workflow.

To achieve this, individual LBM attribution matrices along with the patient matrices (described in Section 3) are visualized using a modular interface that mirrors the way clinicians view the data. The interface contains a chart displaying the patient’s ROM. Also plotted on the same chart is an image representation of the patient’s LBM attribution matrix $M_{1:T}^f$, with time on the x-axis, features on the y-axis. White pixels indicate where $M_t^f = 0$, while red pixels indicate $M_t^f = 1$. Additional charts (scatter plots) of the patient’s data are visualized in alignment with the ROM chart and can be added to or removed from the interface. Furthermore, the clinician can select time windows of interest and compute the average attribution over these time windows. These average attributions are displayed as bar-plots and describe the average importance of each feature in making the prediction over the time windows of interest. An example of visualization is shown in Figure 1.

5 Results

5.1 Patient-Level Attributions

LBM was computed to interpret individual patient ROM predictions generated by the RNN. Presented are examples of two patients in the test dataset with similar ROM predictions but different primary diagnoses. The first is a 1 year old male weighing 10 kg with a primary diagnosis of sepsis (infection); the second is a 14 year old female weighing 74 kg with a primary diagnosis of acute respiratory distress syndrome (ARDS). Both patients do not survive their ICU stay. The ROM predictions for the two patients are shown in Figure 2. In both patients, ROM predictions start low but quickly increase over a short time window, eventually approaching 1. To understand why the model increased its prediction in the highlighted windows, LBM attributions were averaged across each patient using Equation 7: $\overline{M}^{\text{Patient 1}}_{15:20}$ and $\overline{M}^{\text{Patient 2}}_{5:7}$; this is visualized in Figure 3.

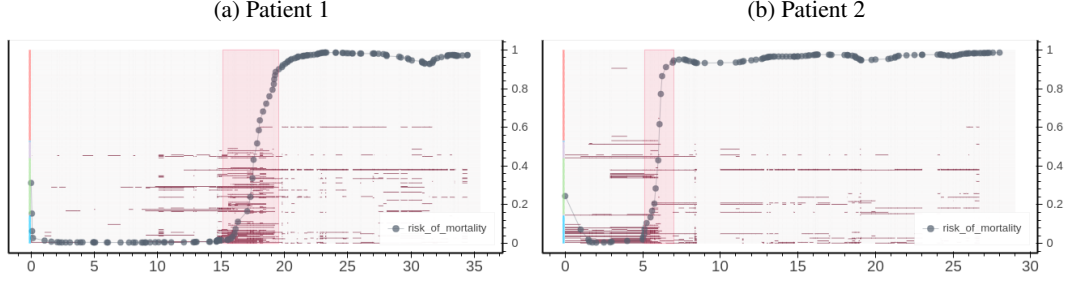


Figure 2: Plotted are ROM predictions over time (in hours). LBM attributions are visualized in the background as an image, with red pixels indicating $M_t^f = 1$ and white pixels indicating $M_t^f = 0$. Red highlighted rectangles are time windows used to compute the average LBM attributions for each patient.

Figure 3 shows that the model used different feature sets for each patient’s prediction: the model’s prediction for Patient 1 used a total of 80/270 (30%) features; while it’s prediction for Patient 2 used 48/270 (18%) features. Clinically the individual sets were consistent with the patients’ primary diagnosis, despite the model knowing no diagnostic information. For example, Patient 1’s top features included Extremity Temperature Level (rank 1), Lactate (rank 10), and features such as Culture Urine (rank 20) which were not used for Patient 2’s prediction during the time window of interest. In contrast, Patient 2’s top features included Respiratory Effort Level (rank 2), FiO2 (rank 3), and features such as EPAP (rank 9) and IPAP (rank 19) which were not used in Patient 1’s predictions during the time window of interest. Although the RNN was optimized to predict whether the patient lives or dies given their physiology and treatments, LBM revealed that the RNN also learned to indirectly model the patho-physiological processes affecting each unique individual: it highlighted infection-associated variables for the patients with sepsis, and respiratory-associated variables for patients with respiratory illness.

5.2 Model “Feature Importance”

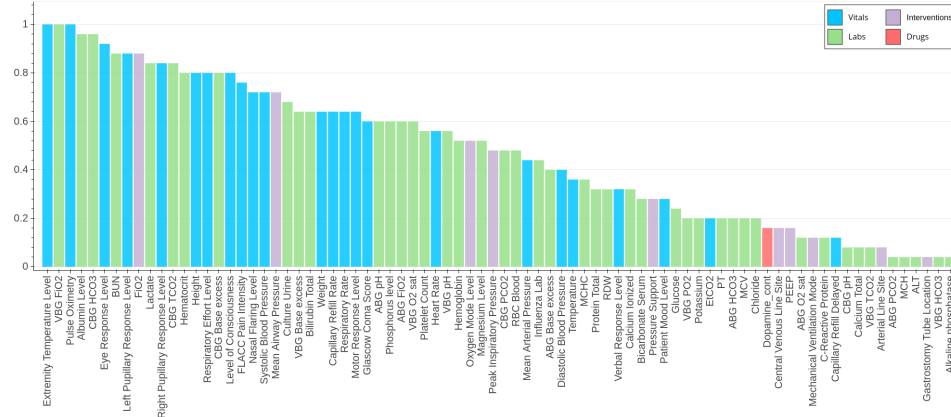
The RNN’s feature importance was obtained as described in 4.3 (Equation 8) and shown in Figure 4. Of the top 10 variables, 6 are qualitative variables manually entered based on the clinician’s judgment (variables with “Level” in the names and Glasgow Coma Score constituents). Moreover, a majority of the top features were clinical observations measured: vitals, labs, age, and gender. This is consistent with previously reported results [28], which showed little performance degradation when variables external to the patients (i.e. interventions and drugs) were excluded as inputs.

This measure of feature importance was further used for feature selection. The top most important 25% features (68/270) were selected and used to train another RNN with the same architecture. Three RNNs were trained with limited features with different weight initializations and mini-batch sequencing. The performance of the limited feature models was compared to the full feature set models, as well as routinely used clinical SOI predictors PIM2 and PRISM3-12 in Figure 5.

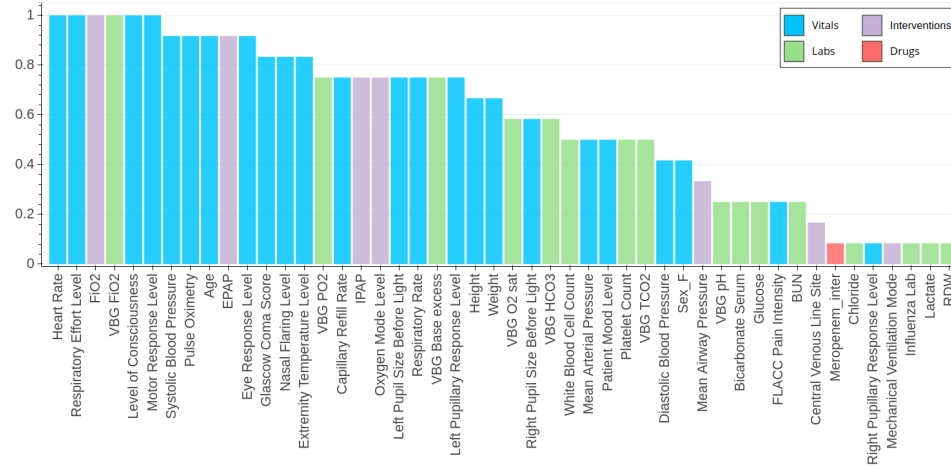
Unlike feature importance extracted from models such as the Random Forest, there is no guarantee that feature selection based on LBM attributions (and thus simply the frequency of use of that feature for making predictions) will maintain or improve predictive performance. Interestingly, the RNN with limited features maintained similar performance with the original model with full 270 features. This is consistent with previous work which showed that including extraneous variables slightly reduced performance [32].

6 Discussion

LBM builds upon the formalization of “meta-predictors” in Fong and Vedaldi [5]. Although it was adapted for an RNN mortality model, the LBM’s formulation is independent of model and data, and thus is applicable to problems outside of time-series data and recurrent neural networks. Because it generates a binary mask, any combination of data-modalities is possible, with proper visualization



(a) Patient 1



(b) Patient 2

Figure 3: Salient features used by the model in making predictions for a) Patient 1 and b) Patient 2 aggregated over each patient’s time windows of interest (see Figure 2). Note that features that do not contribute to the predictions during the time windows of interest are not shown.

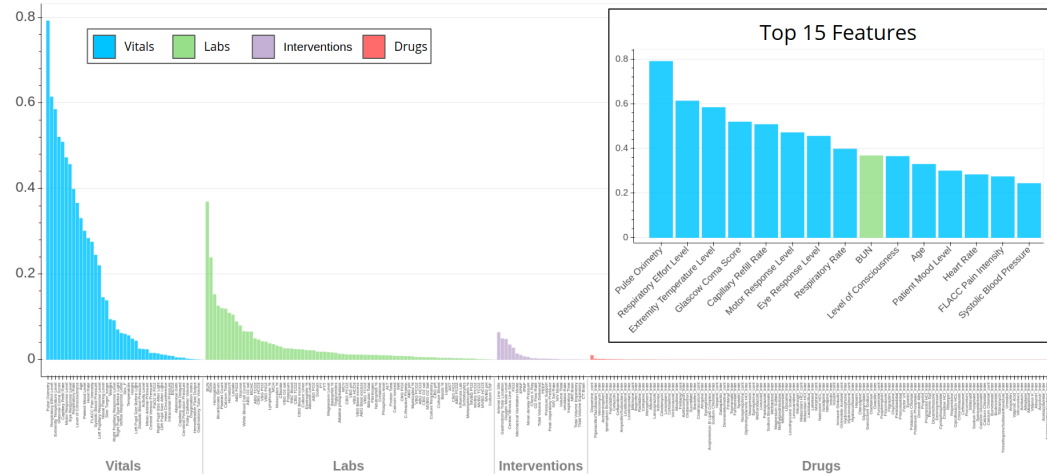


Figure 4: Model “feature importance” computed from LBM attributions, separated by variable types. Also shown in the top right are the top 15 features (top right) no longer separated by variable types.

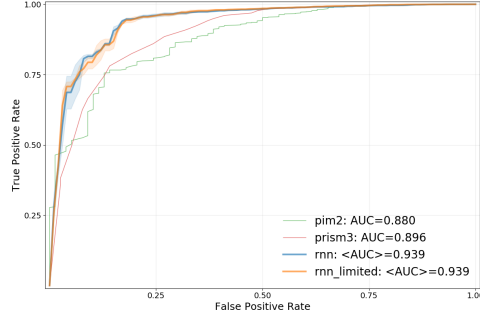


Figure 5: ROC Curves of a RNN trained using all 270 features (rnn_baseline), RNN trained using features selected from LBM’s feature importance (rnn_limited), and two clinical algorithms routinely used in the unit PIM2 and PRISM3-12. Displayed are the average (bold lines) and standard deviation (shaded region) over three iterations for both types of RNN.

and interpretation. Moreover, because it only operates on the inputs and does not utilize layer-specific mechanics, it can be applied to any differentiable neural network model.

LBM has limitations and potential for improvement. It is computationally expensive; it must find an optimal mask for each individual sample of the dataset. Moreover, because LBM solves an optimization problem, there is no guarantee of a unique solution and different hyper-parameters may generate different (and even contradictory) masks. On the other hand, LBM’s sensitivity to hyper-parameters may also be leveraged to improve the algorithm; for example, multiple LBM masks with varying hyperparameters (and thus regularizations) can be applied to a patient’s prediction. These masks can be averaged, generating a real-valued mask (as opposed to binary) where features at each time step are now represented by a "percentage of importance" based on the varying regularization parameters and thus varying masks. To further understand the sensitivity LBM to hyper-parameters, as well as its effectiveness in other problems, future work includes applying and evaluating LBM on additional problems.

In addition to building confidence in the model, LBM can also reveal idiosyncrasies in the model. For example, “Patient Mood Level” is the 12th ranked feature in Figure 4 in making predictions of whether a patient will live or die. The model’s use of this feature may be considered "leakage" of information, depending on the use-case for the model. If the model’s purpose was to only predict ICU mortality, then the qualitative measurement of the patient’s mood should be included. However, if the model’s purpose was to approximate the dynamics of severity of illness based on the patho-physiologic process of the patient’s illness, then the feature should be excluded.

Similar to LBM’s aggregation over the entire dataset to obtain feature importance of the model, LBM attribution matrices can also be aggregated over patient populations to obtain feature importance within cohorts of interest – potentially describing risk factors for mortality across different diseases. However, because diagnoses labels are unreliable [33], a patient may progress through multiple diseases during their ICU stay and attributions averaged over entire ICU encounters may mask significant attributions of each disease and thus cannot be used to easily determine risk factors. With more reliable, time-stamped diagnosis labels, mortality risk factors can easily be obtained; for example, risk factors for the ARDS population can be found by averaging the LBM attributions across each cohort during the annotated time of the diagnosis label.

7 Conclusion

Learned Binary Masks was developed and used to investigate the mechanics of a recurrent model trained to predict an individual patient’s ROM. LBM showed that the model contained clinically-consistent dynamics when determining the patients’ ROM. Moreover, LBM attributions can be aggregated to obtain the model’s “feature importance”. Using this measure of feature importance for feature selection, a limited-feature model using only 25% of the features also performed well.

The method is both data- and model-agnostic and is readily interpretable. Furthermore, it can be aggregated in multiple ways to interpret the model at different scales. Future work includes applying

LBM to additional problems, evaluating its effectiveness in explaining a model’s prediction across different domains, and improving the algorithm.

References

1. Andre Esteva, Alexandre Robicquet, Bharath Ramsundar, Volodymyr Kuleshov, Mark DePristo, Katherine Chou, Claire Cui, Greg Corrado, Sebastian Thrun, and Jeff Dean. A guide to deep learning in healthcare. *Nature medicine*, 25(1):24, 2019.
2. Karen Simonyan, Andrea Vedaldi, and Andrew Zisserman. Deep inside convolutional networks: Visualising image classification models and saliency maps. *arXiv preprint arXiv:1312.6034*, 2013.
3. Matthew D Zeiler and Rob Fergus. Visualizing and understanding convolutional networks. In *European conference on computer vision*, pages 818–833. Springer, 2014.
4. Ramprasaath R Selvaraju, Michael Cogswell, Abhishek Das, Ramakrishna Vedantam, Devi Parikh, and Dhruv Batra. Grad-cam: Visual explanations from deep networks via gradient-based localization. In *Proceedings of the IEEE International Conference on Computer Vision*, pages 618–626, 2017.
5. Ruth C Fong and Andrea Vedaldi. Interpretable explanations of black boxes by meaningful perturbation. In *Proceedings of the IEEE International Conference on Computer Vision*, pages 3429–3437, 2017.
6. Mukund Sundararajan, Ankur Taly, and Qiqi Yan. Axiomatic attribution for deep networks. In *Proceedings of the 34th International Conference on Machine Learning-Volume 70*, pages 3319–3328. JMLR. org, 2017.
7. Chris Olah, Arvind Satyanarayan, Ian Johnson, Shan Carter, Ludwig Schubert, Katherine Ye, and Alexander Mordvintsev. The building blocks of interpretability. *Distill*, 2018. doi: 10.23915/distill.00010. <https://distill.pub/2018/building-blocks>.
8. Chris Olah, Alexander Mordvintsev, and Ludwig Schubert. Feature visualization. *Distill*, 2017. doi: 10.23915/distill.00007. <https://distill.pub/2017/feature-visualization>.
9. Riccardo Guidotti, Anna Monreale, Salvatore Ruggieri, Franco Turini, Fosca Giannotti, and Dino Pedreschi. A survey of methods for explaining black box models. *ACM Comput. Surv.*, 51(5):93:1–93:42, August 2018. ISSN 0360-0300. doi: 10.1145/3236009. URL <http://doi.acm.org/10.1145/3236009>.
10. Benjamin A Goldstein, Ann Marie Navar, Michael J Pencina, and John Ioannidis. Opportunities and challenges in developing risk prediction models with electronic health records data: a systematic review. *Journal of the American Medical Informatics Association*, 24(1):198–208, 2017.
11. Pieter-Jan Kindermans, Sara Hooker, Julius Adebayo, Maximilian Alber, Kristof T Schütt, Sven Dähne, Dumitru Erhan, and Been Kim. The (un) reliability of saliency methods. *arXiv preprint arXiv:1711.00867*, 2017.
12. Jiwei Li, Xinlei Chen, Eduard Hovy, and Dan Jurafsky. Visualizing and understanding neural models in nlp. *arXiv preprint arXiv:1506.01066*, 2015.
13. Andrej Karpathy, Justin Johnson, and Li Fei-Fei. Visualizing and understanding recurrent networks. *arXiv preprint arXiv:1506.02078*, 2015.
14. William A Knaus, Elizabeth A Draper, Douglas P Wagner, and Jack E Zimmerman. Apache ii: a severity of disease classification system. *Critical care medicine*, 13(10):818–829, 1985.
15. Jean-Roger Le Gall, Philippe Loirat, Annick Alperovitch, Paul Glaser, Claude Granthil, Daniel Mathieu, Philippe Mercier, Remi Thomas, and Daniel Villers. A simplified acute physiology score for icu patients. *Critical care medicine*, 12(11):975–977, 1984.

16. Murray M Pollack, Urs E Ruttimann, and Pamela R Getson. Pediatric risk of mortality (prism) score. *Critical care medicine*, 16(11):1110–1116, 1988.
17. F Shann, G Pearson, A Slater, and K Wilkinson. Paediatric index of mortality (pim): a mortality prediction model for children in intensive care. *Intensive care medicine*, 23(2):201–207, 1997.
18. William A Knaus, Douglas P Wagner, Elizabeth A Draper, Jack E Zimmerman, Marilyn Bergner, Paulo G Bastos, Carl A Sirio, Donald J Murphy, Ted Lotring, and Anne Damiano. The apache iii prognostic system. risk prediction of hospital mortality for critically ill hospitalized adults. *Chest Journal*, 100(6):1619–1636, 1991.
19. Rui P Moreno, Philipp GH Metnitz, Eduardo Almeida, Barbara Jordan, Peter Bauer, Riccardo Abizanda Campos, Gaetano Iapichino, David Edbrooke, Maurizia Capuzzo, Jean-Roger Le Gall, et al. Saps 3—from evaluation of the patient to evaluation of the intensive care unit. part 2: Development of a prognostic model for hospital mortality at icu admission. *Intensive care medicine*, 31(10):1345–1355, 2005.
20. Murray M Pollack, Kantilal M Patel, and Urs E Ruttimann. Prism iii: an updated pediatric risk of mortality score. *Critical care medicine*, 24(5):743–752, 1996.
21. Murray M Pollack, Richard Holubkov, Tomohiko Funai, J Michael Dean, John T Berger, David L Wessel, Kathleen Meert, Robert A Berg, Christopher JL Newth, Rick E Harrison, et al. The pediatric risk of mortality score: update 2015. *Pediatric Critical Care Medicine*, 17(1):2–9, 2016.
22. Anthony Slater, Frank Shann, Gale Pearson, PIM Study Group, et al. Pim2: a revised version of the paediatric index of mortality. *Intensive care medicine*, 29(2):278–285, 2003.
23. Lahn Straney, Archie Clements, Roger C Parslow, Gale Pearson, Frank Shann, Jan Alexander, Anthony Slater, ANZICS Paediatric Study Group, the Paediatric Intensive Care Audit Network, et al. Paediatric index of mortality 3: an updated model for predicting mortality in pediatric intensive care. *Pediatric Critical Care Medicine*, 14(7):673–681, 2013.
24. Jean-Roger Le Gall. The use of severity scores in the intensive care unit. *Intensive care medicine*, 31(12):1618–1623, 2005.
25. K Strand and H Flaatten. Severity scoring in the icu: a review. *Acta Anaesthesiologica Scandinavica*, 52(4):467–478, 2008.
26. Jean-Louis Vincent and Rui Moreno. Clinical review: scoring systems in the critically ill. *Critical care*, 14(2):207, 2010.
27. Randall C Wetzel. The ethical imperative of learning from the data. Retrieved from <http://http://ai-med.io/aimed-magazine-02>, pages 58–61, 2018.
28. Long V Ho, David Ledbetter, Melissa Aczon, and Randall Wetzel. The dependence of machine learning on electronic medical record quality. In *AMIA Annual Symposium Proceedings*, volume 2017, page 883. American Medical Informatics Association, 2017.
29. François Chollet et al. Keras. <https://keras.io>, 2015.
30. Tijmen Tieleman and Geoffrey Hinton. Lecture 6.5-rmsprop: Divide the gradient by a running average of its recent magnitude. *COURSERA: Neural networks for machine learning*, 4(2), 2012.
31. Gilles Louppe, Louis Wehenkel, Antonio Sutera, and Pierre Geurts. Understanding variable importances in forests of randomized trees. In *Advances in neural information processing systems*, pages 431–439, 2013.
32. Eugene Laksana, Melissa Aczon, Long Ho, Cameron Carlin, David Ledbetter, and Randall Wetzel. The impact of extraneous variables on the performance of recurrent neural network models in clinical tasks. *arXiv preprint arXiv:1904.01125*, 2019.
33. Jon B Williams, Debjit Ghosh, and Randall C Wetzel. Applying machine learning to pediatric critical care data. *Pediatric Critical Care Medicine*, 19(7):599–608, 2018.

34. Sepp Hochreiter and Jürgen Schmidhuber. Long short-term memory. *Neural computation*, 9(8): 1735–1780, 1997.
35. Xavier Glorot and Yoshua Bengio. Understanding the difficulty of training deep feedforward neural networks. In *Proceedings of the thirteenth international conference on artificial intelligence and statistics*, pages 249–256, 2010.

Appendix A Training, Architecture, and Implementation of RNN

The data were partitioned into 50/25/25 percent splits into train/valid/test sets respectively. The training set (5885 encounters, 4.0% mortality) was used for directly optimizing the RNN weights; the validation set (1962 encounters, 3.9% mortality) was used to select the best performing weights and network hyper-parameters, and the test set (2008 encounters, 4.1% mortality) was used reporting performance. The data were split by *patients*, instead of encounters, to prevent leakage that can result from training and testing on the same *patient*. The label used for training were the outcomes: whether the patient lived or died at the end of their ICU encounter. Because the desired output is many-to-many, the RNN was optimized to predict this label for each time-step.

The particular RNN variant used was the Long Short Term Memory (LSTM) [34]. The network architecture consisted of 3 stacked LSTMs with hidden units 128, 256, 128 and a final fully-connected layer with an output sigmoid activation. Each layer weights were initialized using Glorot uniform [35]. The RNN weights were optimized using RMSprop [30] to minimize the binary cross-entropy loss with an initial learning rate of 10^{-5} and minibatch size of 128. The learning rate was decreased by a factor of 10 if there was no improvement in training loss over 10 epochs. If the learning rate was decimated 3 times or training exceeded 2000 minibatches, the training was terminated.

Appendix B Feature List

Table 1: List of 270 features used for training the RNN model.

Abdominal Girth	Cefazolin_inter	Glasgow Coma Score	Methadone_inter	PT
ABG Base excess	Cefepime_inter	Glucose	Methylprednisolone_inter	PTT
ABG FiO2	Cefotaxime_inter	Glycopyrrolate_inter	Metoclopramide_inter	Pulse Oximetry
ABG HCO3	Ceftriaxime_inter	Head Circumference	Metronidazole_inter	Racemic Epi_inter
ABG O2 sat	Ceftriaxone_inter	Heart Rate	Micafungin_inter	Ranitidine_inter
ABG PCO2	Central Venous Line Site	Height	Midazolam HCL_cont	RBC Blood
ABG pH	Central Venous Pressure	Hematocrit	Midazolam HCL_inter	RDW
ABG PO2	Cerebral Perfusion Pressure	Hemofiltration Fluid Output	Milrinone_cont	Respiratory Effort Level
ABG TCO2	Chest X Ray	Hemoglobin	Monocytes %	Respiratory Rate
Acetaminophen_inter	Chloride	Heparin_cont	Morphine_cont	Rifampin_inter
Acetaminophen/Codeine_inter	Chlorothiazide_inter	Heparin_inter	Morphine_inter	Right Pupil Size After Light
Acetazolamide_inter	Ciprofloxacin HCL_inter	Hydrocortisone_inter	Motor Response Level	Right Pupil Size Before Light
Activity Level	Cisatracurium_cont	Hydromorphone_cont	MRI Brain	Right Pupillary Response Level
Acyclovir_inter	Clindamycin_inter	Hydromorphone_inter	MVBG HCO3	Risperidone_inter
Age	Clonidine HCL_inter	Ibuprofen_inter	MVBG O2 Sat	Rocuronium_inter
Albumin Level	Creatinine	Immune Globulin_inter	MVBG PCO2	Schistocytes
Albumin_inter	CT Brain	Influenza Lab	MVBG pH	Sex_F
Albuterol_inter	Culture Blood	INR	MVBG PO2	Sildenafil_inter
Alkaline phosphatase	Culture CSF	Inspiratory Time	MVBG TCO2	Skin Turgor_turgor
Allopurinol_inter	Culture Respiratory	Insulin_cont	Myelocytes %	Sodium
ALT	Culture Urine	Insulin_inter	Naloxone HCL_inter	Sodium Bicarbonate_inter
Alteplase_inter	Cyclophosphamide_inter	Intracranial Pressure	Nasal Flaring Level	Sodium Chloride_inter
Amikacin_inter	Desmopressin_inter	IPAP	Neutrophils %	Sodium Phosphate_inter
Amphotericin B Lipid Complex_inter	Dexamethasone_inter	Ipratropium Bromide_inter	Nifedipine_inter	Spironolactone_inter
Ampicillin_inter	Dexmedetomidine_cont	Isradipine_inter	NIV Mode	Sucralfate_inter
Ampicillin/Sulbactam_inter	Diastolic Blood Pressure	Ketamine_inter	NIV Set Rate	Systolic Blood Pressure
Arterial Line Site	Diphenhydramine HCL_inter	Ketorolac_inter	Norepinephrine_cont	Temperature
AST	Dopamine_cont	Labetalol_inter	Nystatin_inter	Tidal Volume Delivered
Atropine_inter	Dornase Alfa_inter	Lactate	O2 Flow Rate	Tidal Volume Expiratory
Azithromycin_inter	Eosinophils %	Lactobacillus_inter	Ocoteotide Acetate_cont	Tidal Volume Inspiratory
Baclofen_inter	EPAP	Lansoprazole_inter	Olanzapine_inter	Tobramycin_inter
Bands %	Epinephrine_cont	Left Pupil Size After Light	Ondansetron_inter	Topiramate_inter
Basophils %	Epinephrine_inter	Left Pupil Size Before Light	Oseltamivir_inter	Triglycerides
Bicarbonate Serum	Epoetin_inter	Left Pupillary Response Level	Oxacillin_inter	Trimethoprim/Sulfamethoxazole_inter
Bilirubin Total	EtCO2	Level of Consciousness	Oxycodone_inter	Ursodiol_inter
Budesonide_inter	Extremity Temperature Level	Levetiracetam_inter	Oxygen Mode Level	Valproic Acid_inter
Bumetanide_inter	Eye Response Level	Levocarnitine_inter	Oxygenation Index	Vancomycin_inter
BUN	Factor VII_inter	Levothyroxine Sodium_inter	Pantoprazole_inter	Vasopressin_cont
C-Reactive Protein	Famotidine_inter	Lidocaine_inter	PaO2 to FiO2	VBG Base excess
Calcium Chloride_cont	Fentanyl_cont	Linezolid_inter	Patient Mood Level	VBG FiO2
Calcium Chloride_inter	Fentanyl_inter	Lipase	Peak Inspiratory Pressure	VBG HCO3
Calcium Gluconate_inter	Fibrinogen	Lorazepam_inter	PEEP	VBG O2 sat
Calcium Ionized	Filgrastim_inter	Lymphocyte %	Pentobarbital_inter	VBG PCO2
Calcium Total	FiO2	Magnesium Level	Phenobarbital_inter	VBG pH
Capillary Refill Delayed	FLACC Pain Intensity	Magnesium Sulfate_inter	Phosphorus level	VBG PO2
Capillary Refill Rate	Fluconazole_inter	MCH	Piperacillin/Tazobactam_inter	VBG TCO2
CBG Base excess	Foley Catheter Volume	MCHC	Platelet Count	Vecuronium_inter
CBG FiO2	Fosphenytoin_inter	MCV	Potassium	Ventilator Rate
CBG HCO3	Furosemide_cont	Mean Airway Pressure	Potassium Chloride_inter	Verbal Response Level
CBG O2 sat	Gabapentin_inter	Mean Arterial Pressure	Potassium Phosphate_inter	Vitamin K_inter
CBG PCO2	Ganciclovir Sodium_inter	Mechanical Ventilation Mode	Pressure Support	Volume Tidal
CBG pH	Gastrostomy Tube Location	Meropenem_inter	Propofol_inter	Voriconazole_inter
CBG PO2	Gastrostomy Tube Volume	Metamyleocytes %	Propranolol HCL_inter	Weight
CBG TCO2			Protein Total	White Blood Cell Count